Original article
DOI: https://doi.org/10.18721/JPM.14412

THE INFLUENCE OF HUMAN ARTERIAL NETWORK'S FREQUENCY CHARACTERISTICS ON A PULSE WAVE DELAY ESTIMATION

N. A. Ushakov ✉, *E. A. Semina*, *A. A. Markvart*, *L. B. Liokumovich*

Peter the Great St. Petersburg Polytechnic University, St. Petersburg, Russia

✉ n.ushakoff@spbstu.ru

Abstract: The article has examined the influence of frequency-dependent properties of a human arterial network on the distortion of a pulse wave (PW) signal and a resulting temporary displacement of the slope and systolic peak of the PW signal. When analyzing the operation of a cardiovascular system, a section of the arterial network was simulated by an equivalent *RC* circuit being a low-pass filter. As a result of the simulation, analytical expressions were obtained that allowed to determine the time of the PW signal propagation from a heart to a measuring point. The correctness of the expressions obtained was confirmed by numerical simulation and experimental measurements.

Keywords: pulse wave, transfer function, cardiovascular system, pulse wave delay

Funding: The research was supported by the scholarship of the President of the Russian Federation for young scientists and postgraduates carrying out advanced research and development in priority areas of modernization of the Russian economy for 2021 – 2023. Scholarship No. SP-5631.2021.4.

Citation: Ushakov N. A., Semina E. S., Markvart A. A., Liokumovich L. B. The influence of human arterial network's frequency characteristics on a pulse wave delay estimation, St. Petersburg Polytechnical State University Journal. Physics and Mathematics. 14 (3) (2021) 158–171. DOI: 10.18721/JPM.14412

Научная статья
УДК 612.15
DOI: https://doi.org/10.18721/JPM.14412

ВЛИЯНИЕ ЧАСТОТНЫХ ХАРАКТЕРИСТИК АРТЕРИАЛЬНОЙ СЕТИ ЧЕЛОВЕКА НА ОЦЕНКУ ЗАДЕРЖКИ ПУЛЬСОВОЙ ВОЛНЫ

Н. А. Ушаков ✉, *Е. А. Сёмина*, *А. А. Маркварт*, *Л. Б. Лиокумович*

Санкт-Петербургский политехнический университет Петра Великого, Санкт-Петербург, Россия

✉ n.ushakoff@spbstu.ru

Аннотация. В статье рассмотрено влияние частотно-зависимых свойств артериальной сети человека на искажение сигнала пульсовой волны (ПВ) и результирующее временное смещение склона и систолического пика сигнала ПВ. При анализе функционирования сердечно-сосудистой системы участок артериальной сети моделировали эквивалентной *RC*-цепью, представляющей собой фильтр нижних частот. В результате моделирования получены аналитические выражения, позволяющие найти время распространения сигнала ПВ от сердца до точки измерения ПВ. Корректность полученных выражений подтверждена численным моделированием и экспериментальными измерениями.

Ключевые слова: пульсовая волна, передаточная характеристика, сердечно-сосудистая система, задержка пульсовой волны

Финансирование: Исследование поддержано стипендией Президента Российской Федерации молодым ученым и аспирантам, осуществляющим перспективные научные исследования и разработки по приоритетным направлениям модернизации российской экономики на 2021 – 2023 годы. Стипендия № СП-5631.2021.4.

Для цитирования: Ушаков Н. А., Сёмина Е. А., Маркварт А. А., Лиокумович Л. Б. Влияние частотных характеристик артериальной сети человека на оценку задержки пульсовой волны // Научно-технические ведомости СПбГПУ. Физико-математические науки. 2021. Т. 4 № .14. С. 158–171. DOI: 10.18721/JPM.14412

Introduction

According to the Ministry of Health of the Russian Federation, cardiovascular diseases (CVD) and related complications are the leading cause of mortality in Russia, accounting for almost half of the recorded deaths. About 20% of deaths from CVD occur in the working population. Systematic screening of cardiovascular health and, accordingly, early detection of risk factors, along with healthy diet and lifestyle, is essential for preventing CVD and improving the quality of life in the population.

Most CVD are related to changes in the mechanical properties of cardiac and vascular tissues, namely, a decrease in their elasticity. For this reason, pumping the same blood volume corresponds to a smaller change in the vessel volume, acting to increase the blood pressure and, therefore, the cardiac load. Thus, monitoring the changes in vascular stiffness can help diagnose many CVDs and prevent their severe course. Importantly, the diagnostic technique should be widely available, painless, non-invasive, highly reliable and accurate. Pulse wave analysis (PWA) is one of the most popular approaches, meeting these requirements. A property of the pulse wave (PW) that is easy to interpret is the velocity at which it propagates through blood vessels (PWV). This velocity increases along with the increase in the stiffness of arterial walls, which tends to reduce the delay times between PW signals measured at different points. The carotid and femoral arteries are the most common points for PW measurements, since, on the one hand, they are close to the skin surface, and on the other, they are directly connected to the aorta, thus providing highly representative data.

There are many methods for estimating the delay times between PW signals: the intersecting tangent method [1] is best recognized by the scientific community [2]; however, as we have established in [3], this method is highly susceptible to signal noise, so measurement accuracy and diagnostic reliability may suffer as a result.

Another challenge in estimating PWV and interpreting its values is that the PW signal propagates in the cardiovascular system as a frequency-dependent wave [4–6]. The PWV estimate obtained consequently depends on the heart rate (HR), which means that measurements should be taken at the same HR for correct analysis of the data from cardiac monitoring. The measurement technique is performed in a supine patient who has been at rest for at least 10 minutes. On the other hand, the conditions for PW propagation change during the measurements even in patients at rest due to heart rate variability (HRV) [7], generating inevitable errors in PWV estimates. The intersecting tangent method is reported to have low sensitivity to HRV, but its susceptibility to noise poses a considerable obstacle. Furthermore, as we intend to prove in this study, the PW delay times found by the intersecting tangent method do change depending on HRV due to the semi-empirical nature of the method.

This paper introduces improved methods for finding the PW delay based on analysis of physical and mathematical models of the PW signal and the cardiovascular system. The benefits of the methods proposed are that they have low sensitivity to noise, making it possible to estimate the integral characteristics of the cardiovascular system.

Physical and mathematical model of the cardiovascular system and pulse wave signal

Blood flow in the cardiovascular system (CVS) is caused by periodic contractions of the myocardium, generating increased pressure in the aorta and other arteries extending from it. Due to the length of the arteries, the propagation of the region with elevated pressure bears a wave character. Moreover, because the blood vessels are characterized by such properties as inertance and compliance, a phase shift occurs between the pressure wave and the blood flow wave. In addition, the amplitude of the pressure wave decreases as it travels through the arteries, due to friction of blood against the vessel walls.

As follows from the hydrodynamic description of fluid flow in a tube with elastic walls, the propagation of a pulse wave along the CVS can be clearly translated to an equivalent electrical circuit [8, 9], where voltage corresponds to blood pressure, current to blood flow, electrical resistance to hydrodynamic resistance, capacitance to compliance of vascular walls, inductance to inertance of blood flow. All the laws that are valid for electrical circuits also apply for such an equivalent circuit and can be used for CVS simulations.

Different equivalent models are used for numerical simulation of the CVS, including tens and even hundreds of elements [5, 10, 11]. However, analytical consideration of the CVS is practically impossible with such complex models; for this reason, we are going to adopt a three-element model of the arterial system (Fig. 1). The model comprises such parameters as the characteristic impedance of the arterial network, arterial elasticity, and peripheral resistance. Even though this model is highly simplistic, it still yields predictions of the PW signal that are in good agreement with those observed experimentally [12].

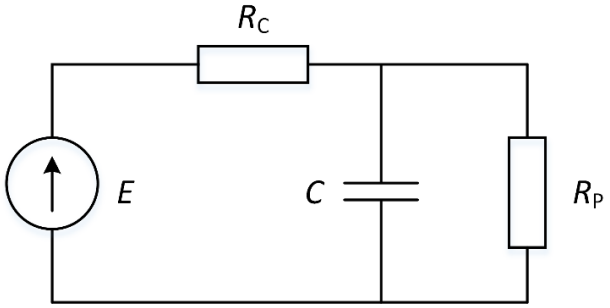

Fig. 1. Three-element equivalent circuit of the arterial network:
R_C, R_p are the resistances of the network vessels and their peripheral system, respectively;
C is the compliance of vascular walls, E is the arterial pressure
generated by the cardiac contraction

Because isovolumic contraction occurs in the myocardium during systole, generating excess pressure, the heart can be described as a voltage source in this simplified model. In turn, the PW sensors whose signals are interpreted to find PWV typically incorporate bioimpedance meters [13, 14], photoplethysmographs [14, 15], and piezoelectric sensors [14, 16], commonly placed over peripheral arteries. Such sensors respond to changes in the volume of blood or tissues surrounding the blood vessel; the flow through the peripheral resistance should therefore be analyzed in the selected equivalent circuit. The same conclusion is true for fiber-optic sensors, showing much promise for recording pulse wave signals [3, 17–20].

While an equivalent lumped-parameter model is used in this study, strictly speaking, the CVS is a system with distributed parameters, which is why secondary (reflected) waves occur in addition to the forward wave generated by cardiac contraction. Secondary waves reflected from the branching points in the arterial network (the reflection is mainly from the aortic branches) are delayed relative to the forward wave. The PW signal has a complex shape as result, with several characteristic peaks and inflection points (see Fig. 2,*a* below).

Mathematical models accounting for reflected waves describe the PW signals with the best accuracy. One of the most accurate models describing the PW signal taking into account the presence of several reflected waves is superposition of Gaussian functions [17, 21]. Signal features (systolic peaks and diastolic dips) are extracted at the first stage; the signal stream is then divided into segments corresponding to individual heartbeats. Diastolic dips act as segment boundaries. The segments extracted by this procedure are then fitted by functions of the form

$$s(t) = \sum_{i=1}^{N} a_i \cdot \exp\left(\frac{\left(t - \tau_{Ai}\right)^2}{\tau_{Ii}^2} \right), \qquad (1)$$

where N is the number of Gaussian functions (typically varying from 3 to 6); the parameters τ_{Ai}, τ_{Ii} and a_i are responsible for the time delay, width and amplitude of the ith term.

Fig. 2,*a* shows a comparison of the PW signal segment and its fit by model (1) with six Gaussian functions.

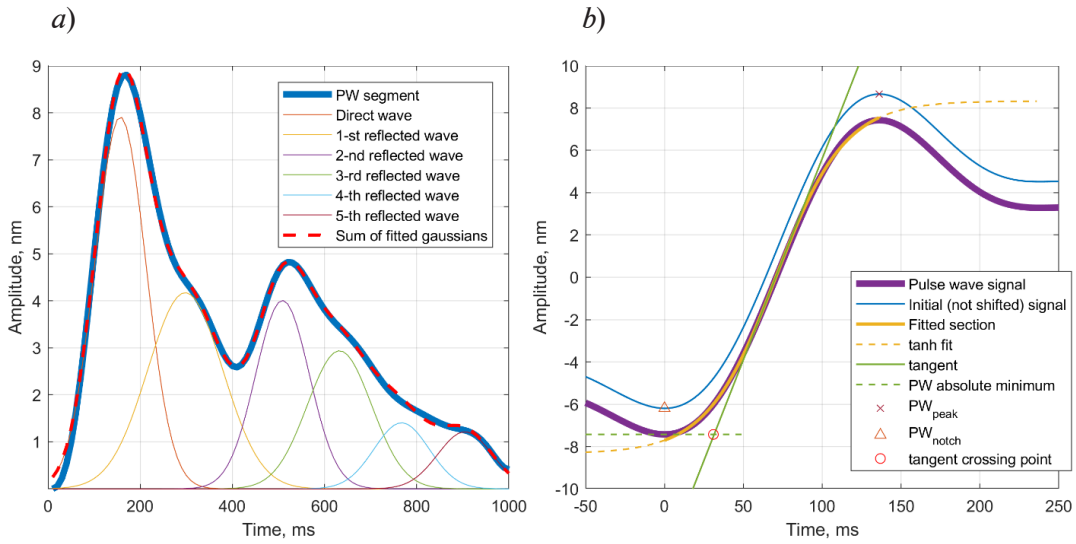

Fig. 2. Examples of PW segment fitted by the multi-Gaussian model (*a*) and systolic peak of this signal fitted by the tanh function (*b*)

Most studies on simulation of the CVS approach it as a linear system. While this assumption is not entirely correct in practice, we also regard the system as linear in this study. Thus, due to additivity, the response of the system to different segments of the perturbation (contraction of the heart muscle) can be considered separately. To simplify the analytical calculations, only the region of the systolic peak with a positive slope was considered in this study, since only a forward wave directly generated by cardiac contraction propagates in this PW segment. This makes the positive slope of the systolic peak extremely interesting for analysis, since the wave behavior in the propagation of arterial wall perturbation can be neglected in this PW segment [22]. Nevertheless, as the positive slope of the systolic peak passes through a part of the arterial network, its shape changes due to the frequency-dependent properties of the CVS: the nature of the changes depends on the properties of the arterial network.

Following the method customarily adopted in the literature (see, for example, [3, 23]), the change in blood pressure during systole is described in this study by the hyperbolic tangent tanh:

$$s(t) = a \cdot \tanh\left(\frac{t - \tau_A}{\tau_I}\right), \tag{2}$$

where the parameters τ_A, τ_I and a, respectively, are responsible for the time delay, time scale and amplitude of the perturbation.

Fig. 2,*b* shows a comparison of the systolic peak region in the PW signal and its positive slope fitted by model (2).

The transmission of signals by the arterial network is described by models (1) or (2) can be studied by finding the impulse response ($h(t)$) and transfer ($H(\omega)$) functions of the equivalent electrical circuit shown in Fig. 1.

Applying the rules for adding resistances in series and parallel connection, given that the impedance of the capacitive element is $1/j\omega t$ (ω is the angular frequency), we can write the transfer function of the equivalent circuit in the form

$$H(\omega) = \frac{R_P}{R_P + R_C + j\omega C R_P R_C}. \tag{3}$$

Applying the inverse Fourier transform to function (3), we find the impulse response of the equivalent circuit in the form

$$h(t) = \frac{1}{CR_C} \exp\left(-\frac{t(R_P + R_C)}{CR_P R_C} \right). \quad (4)$$

Expression (4) for the function $h(t)$ can be rewritten in a more abstract form that is more convenient for analysis:

$$h(t) = \begin{cases} 0, t < 0 \\ b \exp\left(-\frac{t}{\tau_D} \right), t \geq 0 \end{cases}, \quad (5)$$

where τ_D is the time constant of the arterial network, $\tau_D = (C \cdot R_P \cdot R_C)/(R_P + R_C)$; b is the amplitude scaling factor.

Next, the PW signal measured by the sensor $x(t)$ can be found as a convolution of the signal describing the perturbation with the impulse response $h(t)$. Unfortunately, because the shape of the PW signal is distorted, the delay τ_A that is found, for example, by fitting the signal slope by Eq. (2) differs from the true delay. We are going to find the respective corrections in the following section.

Analytical description of pulse wave signals

Calculating the convolution of the Gaussian function in Eqs. (1) and (5) yields the following result:

$$x(t) = \frac{\sqrt{\pi} A}{2} \cdot \exp\left(\frac{\tau_{Ii}^2}{4\tau_D^2} - \frac{t - \tau_{Ai}}{\tau_D} \right) \left[\operatorname{erfc}\left(\frac{\tau_{Ii}^2 - 2t\tau_D + 2\tau_{Ai}\tau_D}{2\tau_D \tau_{Ii}} \right) \right], \quad (6)$$

where erfc is the complementary error function, $\operatorname{erfc}(x) = 1 - \operatorname{erf}(x)$; $A = a_i \cdot b$.

Assuming that the given function (1) describes a forward wave, we can use expression (6) to find the delay of the PW signal passing through the arterial network.

First of all, it should be borne in mind that the time instant τ_{Ai} for signal (1) corresponds to its maximum (it can be found as the zero of the first derivative of signal (6)), while the time instant τ_A for signal (2) corresponds to the inflection point, or the middle of the positive slope (it can be found as the zero of the second derivative of signal (6)).

The first and second derivatives of function (6) should be written as follows:

$$x'(t) = A \exp\left(-\left(\frac{t - \tau_{Ai}}{\tau_{Ii}} \right)^2 \right) - \frac{\sqrt{\pi} A \tau_{Ii}}{\tau_D} \cdot \exp\left(\frac{\tau_{Ii}^2}{4\tau_D^2} - \frac{t - \tau_{Ai}}{\tau_D} \right) \operatorname{erfc}\left(\frac{\tau_{Ii}^2 - 2t\tau_D + 2\tau_{Ai}\tau_D}{2\tau_D \tau_{Ii}} \right); \quad (7)$$

$$x''(t) = A \exp\left(-\left(\frac{t - \tau_{Ai}}{\tau_{Ii}} \right)^2 \right) \cdot \frac{2\tau_{Ai}\tau_D - \tau_{Ii}^2 - 2t\tau_D}{\tau_D \tau_{Ii}^2} + \frac{\sqrt{\pi} A \tau_{Ii}}{2\tau_D^2} \cdot \exp\left(\frac{\tau_{Ii}^2}{4\tau_D^2} - \frac{t - \tau_{Ai}}{\tau_D} \right) \operatorname{erfc}\left(\frac{\tau_{Ii}^2 - 2t\tau_D + 2\tau_{Ai}\tau_D}{2\tau_D \tau_{Ii}} \right). \quad (8)$$

It seems impossible to find the roots of functions (7) and (8) analytically, so we expanded them into a Taylor series in powers of t in the vicinity of the point τ_{Ai}. To obtain the simplest solution, we used the expansion through the linear term of the series.

The resulting linearized functions take the following form:

$$x'_L(t) = \frac{A\left(\tau_D - t + \tau_{Ai}\right)}{2\tau_D^2}\left[2\tau_D - \sqrt{\pi}\tau_{Ii}\cdot\exp\left(\frac{\tau_{Ii}^2}{4\tau_D^2}\right)\mathrm{erfc}\left(\frac{\tau_{Ii}}{2\tau_D}\right)\right]; \tag{9}$$

$$x''_L(t) = \frac{A\left(t - \tau_D - \tau_{Ai}\right)}{2\tau_D^3}\left[2\tau_D - \sqrt{\pi}\tau_{Ii}\cdot\exp\left(\frac{\tau_{Ii}^2}{4\tau_D^2}\right)\mathrm{erfc}\left(\frac{\tau_{Ii}}{2\tau_D}\right)\right] - \\ - \frac{2A\left(t - \tau_{Ai}\right)}{\tau_{Ii}^2} + \frac{A}{\tau_D}. \tag{10}$$

Solving the equations

$$x'_L(t) = 0 \text{ and } x''_L(t) = 0,$$

we obtain the following expressions for the positions of the signal peak τ'_{Ai} and the inflection point τ'_A:

$$\tau'_{Ai} = \tau_{Ai} + \tau_D, \tag{11}$$

$$\tau'_A = \tau_{Ai} + \tau_D - \frac{4\tau_D^2}{4\tau_D^3 - 2\tau_D\tau_{Ii}^2 - \sqrt{\pi}\tau_{Ii}^3\cdot\exp\left(\frac{\tau_{Ii}^2}{4\tau_D^2}\right)\mathrm{erfc}\left(\frac{\tau_{Ii}}{2\tau_D}\right)}. \tag{12}$$

Thus, Eqs. (11) and (12) can be used to accurately find the true arrival time τ_{Ai} of the PW signal after we find its properties and the time constant of the arterial section connecting the heart to the point where the PW is measured. The arrival time τ_{Ai} found by Eqs. (11) and (12) corresponds to the wave peak; it is generally more convenient to deal with the position of the steepest part of the slope or the foot of the wave. If the tanh function is taken to describe the positive slope of the systolic peak more accurately, then the inflection point coincides with the middle of the slope. For a Gaussian function, this point can be found from the condition

$$\exp(-(t - \tau_{Ai})^2/\tau_I^2) = 1/2,$$

yielding the following solution:

$$\tau_A = \tau_{Ai} - \sqrt{-\ln(1/2)}\tau_I. \tag{13}$$

However, the convolution integral of functions (2) and (5) cannot be taken analytically; therefore, the transformation of the pressure wave described by Eq. (2) for the CVS with impulse response (5) was found by numerical calculations.

Numerical simulation of the pulse wave signal and finding its parameters

All numerical calculations in this study were performed in the MATLAB software package. To simulate the PW signal measured by the sensor $x(t)$, we first calculated the initial signal $s(t_i)$ by Eq. (2) with the parameter values $\tau_A = 0$, $\tau_I = 1$ and $a = 1$ in the interval $-5 < t_i < 5$ with the sampling rate $\delta t = t_{i+1} - t_i = 0.01$. The impulse responses $h(t_i)$ were also calculated by Eq. (5) with the parameters $0.1 < \tau_D < 10$ and $b = 1$ in the interval $0 < t_i < 10$ with the sampling rate $\delta t = 0.01$. Thus, 991 arrays containing the values of the function $h(t_i)$ were calculated, each corresponding to a specific τ_D. The PW signal measured by the sensor was simulated by applying a convolution operation to the arrays of perturbation and impulse response; an array of reference PW signal values $x(t_i)$ was calculated for each τ_D.

Because the CVS model used is essentially a low-pass filter, the signal $x(t_i)$ differs in shape from the initial signal $s(t_i)$, so that the degree of difference grows with the increase in the time constant τ_D (equivalent to a decrease in the cut-off frequency of the filter with a constant

signal slope). As our main goal was to determine the degree of distortion introduced into the signal by the arterial network, finding the most accurate method to estimate the arrival time of the PW signal τ_A, we fitted the modeled signals $x(t_i)$ by Eq. (2) using the least squares method. The fitting provided the parameters of the simulated PW signal τ'_A, τ'_I and a', as well as the standard deviation (SD) σ_R.

The parameter we are focusing on in this study is the arrival time of the measured PW signal τ'_A and its relationship with the true arrival time τ_A. Establishing this relationship is relatively complicated, since both the parameters of the initial signal and the parameters of the arterial network are unknown. An additional parameter σ_R was included in the analysis to overcome this difficulty. The dependences of the obtained parameters of the PW signal τ_D, τ'_A and τ'_I on the standard deviation σ_R normalized by the amplitude a' were analyzed and approximated by analytical expressions. The resulting dependences were approximated by the following analytical expressions:

$$\tau_D = p_1\sigma_R^{p_2} + p_3\sigma_R^{p_4}, \tag{14}$$

$$\tau'_A = q_1\sigma_R^{q_2} + q_3\sigma_R^{q_4}, \tag{15}$$

$$\tau'_I = 1 + r_1\sigma_R^{r_2} + r_3\sigma_R^{r_4}, \tag{16}$$

where $p_1 = 11$, $p_2 = 0.52$, $p_3 = 8392$, $p_4 = 2.61$; $q_1 = 9.25$, $q_2 = 0.5$, $q_3 = 7964$, $q_4 = 2.66$; $r_1 = 30.81$, $r_2 = 0.9$, $r_3 = 18070$, $r_4 = 2.99$.

The fitting curves almost completely correspond to the dependences obtained by numerical simulation, which is confirmed by the values of the determination coefficients R^2, turning out to be equal to 0.995, 0.997 and 0.994 for expressions (14), (15) and (16), respectively.

The argument of the tanh function, which was used to approximate the measured PW signal, takes the form

$$t' = \frac{t - \tau'_A}{\tau'_I} = \frac{t - \tau_A - \delta\tau_A}{\tau_I \cdot k_t}. \tag{17}$$

Imposing the condition that the right-hand and left-hand sides of Eq. (17) be equal, and tailoring the parameter values of the initial signal $\tau_A = 0$ and $\tau_I = 1$, we obtain the following relation connecting the parameters of the initial and measured signals:

$$\delta\tau_A = \tilde{\tau}_A \cdot \tau'_I,\ \tilde{\tau}_I = k_t,$$

where the parameters $\tilde{\tau}_A$ and $\tilde{\tau}_I$ can be found from the fitting models (15) and (16), based on the value of the normalized SD (σ_R/a').

As a result, the true arrival time of the PW signal can be defined as

$$\tau_A = \tau'_A - \tilde{\tau}_A \cdot \tau'_I, \tag{18}$$

Another interesting parameter for analysis is the positive slope duration τ_I of the systolic peak, which, in accordance with Eq. (17), can be expressed as

$$\tau_I = \frac{\tau'_I}{\tilde{\tau}_I}. \tag{19}$$

Thus, simulation of the PW signals yielded the results making it possible to determine the time constant for a section of the arterial network and use these data to correct the arrival time of the PW signal found by fitting with Gaussian functions of the form (1) and the hyperbolic tangent of the form (2).

Additional calculations were carried out to verify whether the derivations and the numerical simulation results obtained were correct. The PW signal was given as a superposition of six Gaussian functions of the form (1), while the values of the parameters τ_{Ai}, τ_{Ii} and a_i

for i = 1, 2, ..., 6 were obtained by fitting a segment of the PW signal measured in the carotid artery of a healthy volunteer by the corresponding model superposing six functions of the form (1). The measurement technique is described in our earlier paper [3]. To reproduce the real situation more accurately, we simulated 100 segments of the PW signal, obtaining the values of the parameters τ_{Ai}, τ_{Ii} and a_i for each segment from different segments of the experimental PW signal corresponding to individual heartbeats. The sampling rate of the simulated signals was 1 kHz, the duration of each signal segment was selected equal to 1 s. A low-pass filter with a cutoff frequency varied from 500 to 10 Hz was then applied to the signals calculated by this procedure (this interval corresponds to the filter time constant varying within the range from 2 to 100 ms). The arrival times $\tau\rangle_A$ and τ'_{A1} were found for the obtained set of filtered signals fitting the slopes with functions (2) and full signal segments with functions (1), respectively. The arrival times of the initial, unfiltered signal τ_A, which were used as reference values for verifying the method chosen for estimating the arrival time of the PW signal, were found similarly. Fig. 3 shows the arrival times of the filtered signal depending on the filter time constant for the arrival times found by different methods. Evidently, the expressions (11), (12) and (18) that we obtained for finding the arrival time period combined with the estimate of the filter time constant (14) considerably reduce the error in determining the required value compared with the direct estimate $\tau\rangle_A$, also yielding greater accuracy than the conventional intersecting tangent method.

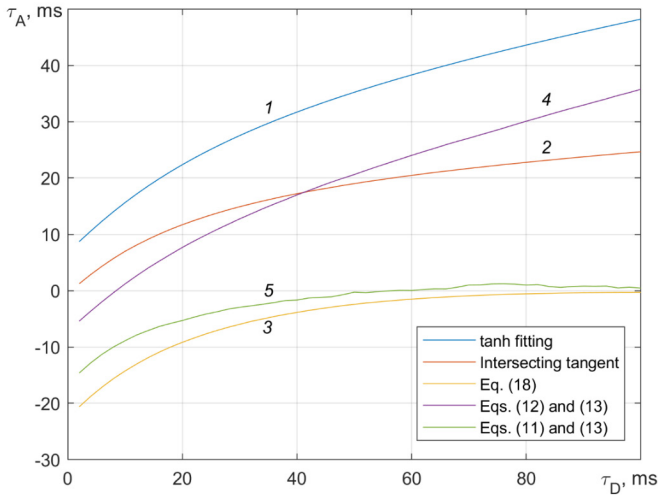

Fig. 3. Arrival times of PW signal
found by different methods depending on the rise time constant
of impulse response in the arterial network.
The arrival time of the PW signal was estimated by: fitting the slopes with function (2) (curve *1*);
the intersecting tangent method (curve *2*); adjusting the values of curve *1* by Eq. (18) (curve *3*);
by Eqs. (12) and (13) (curve *4*); by Eqs. (11) and (13) (curve *5*)

Experimental verification of the proposed methods for finding the delay of the pulse wave signal

In addition to numerical simulation described above, we carried out experimental studies to test the proposed methods for finding the arrival times of the PW signal. To this end, we recruited two volunteers, measuring the pulse wave at their wrists and ankles (the radial and tibial arteries, respectively). PW signals were measured with two multiplexed fiber-optic Fabry–Perot interferometers. The optical path difference of the interferometers changed under the action of the pulse wave, which we recorded using spectral interferometry and the corresponding methods for signal demodulation. A detailed description of the measuring setup and measurement technique is given in [3].

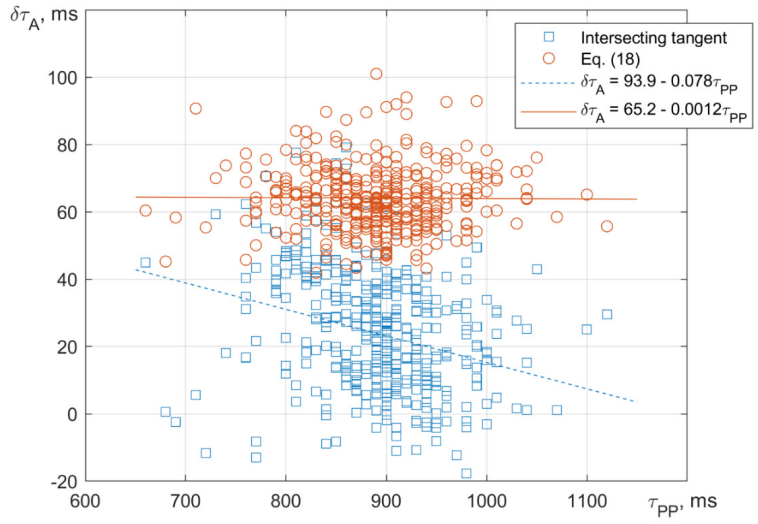

Fig. 4. Experimental points (symbols) and fitting straight lines reflecting the PW signal delay between the wrist and ankle depending on the time interval between heart beats for two experimental processing methods: intersecting tangent (red symbols) and our method determining the slope positions with corrections by Eq. (18) (blue symbols)

The delay between PW signals measured in different arteries served as a criterion indicating that the proposed methods were correct. Due to the frequency-dependent nature of PW propagation in the arterial network, the existing methods for finding the PW delay can produce inaccurate readings that turn out to be correlated with the heart rate even given small changes induced by HRV. At the same time, precise methods minimizing the effect of the frequency spectrum of the PW signal on finding the delay should provide PW delay readings independent of the heart rate.

Fig. 4 shows the dependences of the delay between the pulse wave signals measured at the wrists and at the ankles, where the delay was estimated by the intersecting tangent method, fitting the systolic slope of the PW signal by function (2) and correction of the signal by Eq. (18).

Furthermore, we found the delay between the PW signals by fitting the PW signal segments with models of the form (1), with subsequent correction using Eqs. (11) and (13), however, since the deviations from the values obtained from expression (18) were extremely small, they are not shown in the graphs. The values obtained by fitting the PW slope with Eq. (2) without correction are not shown either (for reading convenience), since they have an even more pronounced dependence than the values obtained by the intersecting tangent method. The fits of the obtained dependences by equations of straight lines are also shown. As evident from Fig. 4, the errors in determining the delay of the PW signal are almost completely compensated with the proposed method, which will make it possible to use the physical and mathematical techniques developed for high-precision processing of PW signals in medical diagnostics and in research.

Conclusion

We have carried out theoretical analysis of the influence that the frequency characteristics of the arterial network have on the conditions of pulse wave propagation, proposing a method for assessing the frequency characteristics in a section of the arterial network. We have obtained analytical expressions for finding the arrival time of the PW signal by fitting the slopes of systolic peaks by the hyperbolic tangent function (tanh) and the PW signal fragments by the multi-Gaussian model. The proposed approaches offer high accuracy for finding the arrival time of the PW signal: this is confirmed by numerical simulation and by processing the experimental PW signals.

REFERENCES

1. **Hermeling E., Reesink K. D., Reneman R. S., Hoeks A. P. G.,** Measurement of local pulse wave velocity: effects of signal processing on precision, Ultrasound Med. Biol. 33 (5) (2007) 774–781.

2. **Wilkinson I. B., McEniery C., Schillaci G., et al.,** ARTERY Society guidelines for validation of non-invasive haemodynamic measurement devices: Part 1, Arterial pulse wave velocity, Artery Res. 4 (2) (2010) 34–40.

3. **Ushakov N. A., Markvart A. A., Liokumovich L. B.,** Pulse wave velocity measurement with multiplexed fiber optic Fabry – Perot interferometric sensors, IEEE Sens. J. 20 (19) (2020) 11302–11312.

4. **Tan I., Butlin M., Spronck B., et al.,** Effect of heart rate on arterial stiffness as assessed by pulse wave velocity, Curr. Hypertens. Rev. 14 (2) (2018) 107–122.

5. **Xiao H., Butlin M., Tan I., Avolio A.,** Effects of cardiac timing and peripheral resistance on measurement of pulse wave velocity for assessment of arterial stiffness, Sci. Rep. 7 (1) (2017) 1–10.

6. **Papaioannou G., Oikonomou E., Lazaros G., et al.,** The influence of resting heart rate on pulse wave velocity measurement is mediated by blood pressure and depends on aortic stiffness levels: Insights from the Corinthia study, Physiol. Meas. 40 (5) (2019) 055005.

7. **Malik M., Bigger J. T., Camm A. J., et al.,** Heart rate variability: Standards of measurement, physiological interpretation, and clinical use, Circulation. 93 (5) (1996) 1043–1065.

8. **Westerhof N., Noordergraaf A.,** Arterial viscoelasticity: A generalized model: Effect on input impedance and wave travel in the systematic tree, J. Biomech. 3 (3) (1970) 357–379.

9. **Jager G. N., Westerhof N., Noordergraaf A.,** Oscillatory flow impedance in electrical analog of arterial system: Representation of sleeve effect and non-Newtonian properties of blood, Circ. Res. 16 (2) (1965) 121–133.

10. **Avolio A. P.,** Multi-branched model of the human arterial system, Med. Biol. Eng. Comput. 18 (6) (1980) 709–718.

11. **Heldt T., Mukkamala R., Moody G. B., Mark R. G.,** CVSim: An open-source cardiovascular simulator for teaching and research, Open Pacing, Electrophysiol. Ther. J. 2010. Vol. 3 (January) (2010) 45–54.

12. **Stergiopulos N., Westerhof B. E., Westerhof N.,** Total arterial inertance as the fourth element of the windkessel model, Am. J. Physiol. Heart Circ. Physiol. 276 (1) (1999) H81–H88.

13. **Kusche R., Klimach P., Ryschka M.,** A multichannel real-time bioimpedance measurement device for pulse wave analysis, IEEE Trans. Biomed. Circuits Syst. 12 (3) (2018) 614–622.

14. **Pielmuş A.-G., Osterland D., Klum M., et al.,** Correlation of arterial blood pressure to synchronous piezo, impedance and photoplethysmographic signal features, Curr. Dir. Biomed. Eng. 3 (2) (2017) 749–753.

15. **Moço A. V., Stuijk S., de Haan G.,** New insights into the origin of remote PPG signals in visible light and infrared, Sci. Rep. 8 (May 31) (2018) 8501.

16. **Vardoulis O., Saponas T.S., Morris D., et al.,** In *vivo* evaluation of a novel, wrist-mounted arterial pressure sensing device versus the traditional hand-held tonometer, Med. Eng. Phys. 38 (10) (2016) 1063–1069.

17. **Ushakov N., Markvart A., Kulik D., Liokumovich L.,** Comparison of pulse wave signal monitoring techniques with different fiber-optic interferometric sensing elements, Photonics. 8 (5) (2021) 142.

18. **Wang J., Liu K., Sun Q., et al.,** Diaphragm-based optical fiber sensor for pulse wave monitoring and cardiovascular diseases diagnosis, J. Biophotonics. 12 (10) (2019) e201900084.

19. **Domingues M. F., Tavares C., Alberto N., et al.,** High rate dynamic monitoring with Fabry – Perot interferometric sensors: An alternative interrogation technique targeting biomedical applications, Sensors. 19 (21) (2019) 4744.

20. **Haseda Y., Bonefacino J., Tam H.-Y., et al.,** Measurement of pulse wave signals and blood pressure by a plastic optical fiber FBG sensor, Sensors. 19 (23) (2019) 5088.

21. **Couceiro R., Carvalho P., Paiva R. P., et al.,** Assessment of cardiovascular function from multi-Gaussian fitting of a finger photoplethysmogram, Physiol. Meas. 36 (9) (2015) 1801–1826.

22. **Li J. K. J.,** Time domain resolution of forward and reflected waves in the aorta, IEEE Trans. Biomed. Eng. BME-33 (8) (1986) 783–785.

23. **Sola J., Vetter R., Renevey P., et al.,** Parametric estimation of pulse arrival time: A robust approach to pulse wave velocity, Physiol. Meas. 30 (7) (2009) 603–615.

СПИСОК ЛИТЕРАТУРЫ

1. **Hermeling E., Reesink K. D., Reneman R. S., Hoeks A. P. G.** Measurement of local pulse wave velocity: effects of signal processing on precision // Ultrasound Medicine and Biology. 2007. Vol. 33. No. 5. Pp. 774–781.

2. **Wilkinson I. B., McEniery C., Schillaci G., Boutouyrie P., Segers P., Donald A., Chowienczyk Ph. J.** ARTERY Society guidelines for validation of non-invasive haemodynamic measurement devices: Part 1, Arterial pulse wave velocity // Artery Research. 2010. Vol. 4. No. 2. Pp. 34–40.

3. **Ushakov N. A., Markvart A. A., Liokumovich L. B.** Pulse wave velocity measurement with multiplexed fiber optic Fabry – Perot interferometric sensors // IEEE Sensors Journal. 2020. Vol. 20. No. 19. Pp. 11302–11312.

4. **Tan I., Butlin M., B. Spronck B., Xiao H., Avolio A.** Effect of heart rate on arterial stiffness as assessed by pulse wave velocity // Current Hypertension Reviews. 2018. Vol. 14. No. 2. Pp. 107–122.

5. **Xiao H., Butlin M., Tan I., Avolio A.** Effects of cardiac timing and peripheral resistance on measurement of pulse wave velocity for assessment of arterial stiffness // Scientific Reports. 2017. Vol. 7. No. 1. Pp. 1–10.

6. **Papaioannou G., Oikonomou E., Lazaros G., et al.** The influence of resting heart rate on pulse wave velocity measurement is mediated by blood pressure and depends on aortic stiffness levels: Insights from the Corinthia study // Physiological Measurement. 2019. Vol. 40. No. 5. P. 055005.

7. **Malik M., Bigger J. T., Camm A. J., Kleiger R. E., Malliani A., Moss A. J., Schwartz P. J.** Heart rate variability: Standards of measurement, physiological interpretation, and clinical use // Circulation. 1996. Vol. 93. No. 5. Pp. 1043–1065.

8. **Westerhof N., Noordergraaf A.** Arterial viscoelasticity: A generalized model: Effect on input impedance and wave travel in the systematic tree // Journal of Biomechanics. 1970. Vol. 3. No. 3. Pp. 357–379.

9. **Jager G. N., Westerhof N., Noordergraaf A.** Oscillatory flow impedance in electrical analog of arterial system: Representation of sleeve effect and non-Newtonian properties of blood // Circulation Research. 1965. Vol. 16. No. 2. Pp. 121–133.

10. **Avolio A. P.** Multi-branched model of the human arterial system // Medical & Biological Engineering & Computing. 1980. Vol. 18. No. 6. Pp. 709–718.

11. **Heldt T., Mukkamala R., Moody G. B., Mark R. G.** CVSim: An open-source cardiovascular simulator for teaching and research // The Open Pacing, Electrophysiology & Therapy Journal. 2010. Vol. 3. January. Pp. 45–54.

12. **Stergiopulos N., Westerhof B. E., Westerhof N.** Total arterial inertance as the fourth element of the windkessel model // American Journal of Physiology – Heart and Circulatory Physiology. 1999. Vol. 276. No. 1. Pp. H81–H88.

13. **Kusche R., Klimach P., Ryschka M.** A multichannel real-time bioimpedance measurement device for pulse wave analysis // IEEE Transactions on Biomedical Circuits & Systems. 2018. Vol. 12. No. 3. Pp. 614–622.

14. **Pielmuş A.-G., Osterland D., Klum M., et al.** Correlation of arterial blood pressure to synchronous piezo, impedance and photoplethysmographic signal features // Current Directions in Biomedical Engineering. 2017. Vol. 3. No. 2. Pp. 749–753.

15. **Moço A. V., Stuijk S., de Haan G.** New insights into the origin of remote PPG signals in visible light and infrared // Scientific Reports. 2018. Vol. 8. May 31. P. 8501.

16. **Vardoulis O., Saponas T.S., Morris D., Villar N., Smith G., Patel S., Desney T.** In *vivo* evaluation of a novel, wrist-mounted arterial pressure sensing device versus the traditional hand-held tonometer // Medical Engineering & Physics. 2016. Vol. 38. No. 10. Pp. 1063–1069.

17. **Ushakov N., Markvart A., Kulik D., Liokumovich L.** Comparison of pulse wave signal monitoring techniques with different fiber-optic interferometric sensing elements // Photonics. 2021. Vol. 8. No. 5. P. 142.

18. **Wang J., Liu K., Sun Q., Ni X., Ai F., Wang S., Yan Z., Liu D.** Diaphragm-based optical fiber sensor for pulse wave monitoring and cardiovascular diseases diagnosis // Journal of Biophotonics. 2019. Vol. 12. No. 10. P. e201900084.

19. **Domingues M. F., Tavares C., Alberto N., Radwan A., Andrй P., Antunes P.** High rate dynamic monitoring with Fabry – Perot interferometric sensors: An alternative interrogation technique targeting biomedical applications // Sensors. 2019. Vol. 19. No. 21. P. 4744.

20. **Haseda Y., Bonefacino J., Tam H.-Y., Chino S., Koyama S., Ishizawa H.** Measurement of pulse wave signals and blood pressure by a plastic optical fiber FBG sensor // Sensors. 2019. Vol. 19. No. 23. P. 5088.

21. **Couceiro R., Carvalho P., Paiva R. P., et al.** Assessment of cardiovascular function from multi-Gaussian fitting of a finger photoplethysmogram // Physiological Measurement. 2015. Vol. 36. No. 9. Pp. 1801–1826.

22. **Li J. K. J.** Time domain resolution of forward and reflected waves in the aorta // IEEE Transactions on Biomedical Engineering. 1986. Vol. BME-33. No. 8. Pp. 783–785.

23. **Sola J., Vetter R., Renevey P., Chételat O., Sartori C., Rimoldi S. F.** Parametric estimation of pulse arrival time: A robust approach to pulse wave velocity // Physiological Measurement. 2009. Vol. 30. No. 7. Pp. 603–615.

THE AUTHORS

USHAKOV Nikolai A.
Peter the Great St. Petersburg Polytechnic University
29 Politechnicheskaya St., St. Petersburg, 195251, Russia
n.ushakoff@spbstu.ru
ORCID: 0000-0002-3480-2779

SEMINA Ekaterina A.
Peter the Great St. Petersburg Polytechnic University
29 Politechnicheskaya St., St. Petersburg, 195251, Russia
feanaara@gmail.com
ORCID: 0000-0003-0389-5578

MARKVART Aleksandr A.
Peter the Great St. Petersburg Polytechnic University
29 Politechnicheskaya St., St. Petersburg, 195251, Russia
markvart_aa@spbstu.ru
ORCID: 0000-0001-8080-0830

LIOKUMOVICH Leonid B.
Peter the Great St. Petersburg Polytechnic University
29 Politechnicheskaya St., St. Petersburg, 195251, Russia
leonid@spbstu.ru
ORCID: 0000-0001-5988-1429

СВЕДЕНИЯ ОБ АВТОРАХ

УШАКОВ Николай Александрович – *кандидат физико-математических наук, доцент Высшей школы прикладной физики и космических технологий Санкт-Петербургского политехнического университета Петра Великого.*
195251, Россия, г. Санкт-Петербург, Политехническая ул., 29
n.ushakoff@spbstu.ru
ORCID: 0000-0002-3480-2779

СЁМИНА Екатерина Александровна – *инженер Высшей школы прикладной физики и космических технологий Санкт-Петербургского политехнического университета Петра Великого.*
195251, Россия, г. Санкт-Петербург, Политехническая ул., 29
feanaara@gmail.com
ORCID: 0000-0003-0389-5578

МАРКВАРТ Александр Александрович – *ассистент Высшей школы прикладной физики и космических технологий Санкт-Петербургского политехнического университета Петра Великого.*
195251, Россия, г. Санкт-Петербург, Политехническая ул., 29
markvart_aa@spbstu.ru
ORCID: 0000-0001-8080-0830

ЛИОКУМОВИЧ Леонид Борисович – *доктор физико-математических наук, профессор Высшей школы прикладной физики и космических технологий Санкт-Петербургского политехнического университета Петра Великого.*
195251, Россия, г. Санкт-Петербург, Политехническая ул., 29
leonid@spbstu.ru
ORCID: 0000-0001-5988-1429

Received 26.10.2021. Approved after reviewing 14.11.2021. Accepted 14.11.21.
Статья поступила в редакцию 26.10.2021. Одобрена после рецензирования 14.11.2021. Принята 14.11.21.